Review Article **Open Access**

Yun-Han Lee, Guanjun Tan, Tao Zhan, Yishi Weng, Guigeng Liu, Fangwang Gou, Fenglin Peng, Nelson V. Tabiryan, Sebastian Gauza, and Shin-Tson Wu*

Recent progress in Pancharatnam–Berry phase optical elements and the applications for virtual/augmented realities

DOI 10.1515/odps-2017-0010
Received June 1, 2017; accepted June 5, 2017

Abstract: In this review paper, we report recent progress on Pancharatnam–Berry (PB) phase optical elements, such as lens, grating, and deflector. PB lenses exhibit a fast switching time between two or more focal lengths with large diopter change and aperture size, which is particularly attractive for addressing the accommodation mismatch in head-mounted display devices. On the other hand, PB gratings and deflectors offer a large-angle beam deflection with wide acceptance cone and high efficiency, as compared to conventional volume gratings. Such merits provide great advantages for waveguide-coupling augmented reality headsets. Moreover, the thickness of PB optical elements is only a few micrometers, thus they can be conveniently integrated into modern wearable display systems.

Keywords: Liquid-crystal devices; Lens system design

1 Introduction

Due to the rapid development of small-size yet high-resolution display panels and unprecedented computing power of modern computers, portable devices with versatile functionalities are now ubiquitous. The realization of virtual reality (VR) and augmented reality (AR) are coming to actual reality. Among the several remaining challenges, the depth perception is gaining more and more attention. As shown in Fig. 1(a), in a binocular AR/VR device, three-dimensional (3D) perception is provided through the stereopsis, where two images from different viewing points are sent to different eyes. The mismatch between stereopsis and accommodation (eye's focal distance) cues in a VR headset is one of the reasons causing *VR sickness*. In AR, the mismatch between displayed image and real environment renders it difficult for the user to see the displayed image.

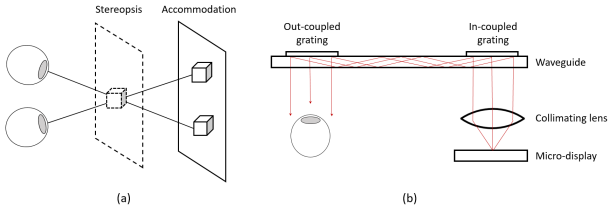

Figure 1: (a) The mismatch between the stereopsis cue and the accommodation cue in a VR headset. (b) A common waveguide setup for an AR glass, showing only one eye.

Several approaches have been proposed to accommodate the displayed distance, such as integral displays [1, 2], light field displays [3–5] and depth-fused displays [6, 7]. In an integral display, microlens array is used to project different images to different perspectives and thus form a sense of depth. However, this method reduces the resolution of the display, which is not acceptable in many cases. To retain the resolution, a depth-fused display projects the objects to different depths (distances) rapidly and forms a superposed image distance by modulating the relative intensity of the image. This approach requires switching between at least 5 distances [7] and therefore a fast switching lens and a fast-response display panel are required. For example, to obtain a 60-Hz display, minimally it re-

***Corresponding Author: Shin-Tson Wu:** CREOL, The College of Optics and Photonics, University of Central Florida, Orlando, Florida 32816, USA, E-mail: swu@ucf.edu
Yun-Han Lee, Guanjun Tan, Tao Zhan, Fangwang Gou, Fenglin Peng: CREOL, The College of Optics and Photonics, University of Central Florida, Orlando, Florida 32816, USA
Yishi Weng: School of Electronic Science and Engineering, Southeast University, Nanjing 210018, China
Guigeng Liu: School of Physics, Nankai University, Tianjin 300071, China
Nelson V. Tabiryan: Beam Engineering for Advanced Measurements Co., Orlando, Florida 32810, USA
Sebastian Gauza: LC Matter Corp., Orlando, Florida 32816, USA

quires a 300-Hz display with a switchable lens much faster than 3.3 ms. Light field display, on the other hand, computes appropriate display image at different distances to reconstruct an approximated 3D light field. For a 2-panel time-multiplexed additive light field display at 60 Hz, it will require a 120-Hz display with a switchable lens whose response time is much faster than 8.3 ms. The displayed signal during lens switching process will inevitably result in degraded quality; therefore, in all cases, it is not only desirable but critical to utilize a fast-switching lens. Several approaches have been proposed to realize focal length switching [8–13]; however, these devices are either slow in response time (>5 ms) or very difficult to integrate into small form-factor, and thus cannot meet the strict requirements of a compact and lightweight wearable display device. These all together raise the need for a fast, compact switchable lens with large aperture, which can be realized with Pancharatnam–Berry lenses (PBLs) as described in the following section.

For augmented reality (AR) devices, an extra combiner is required to integrate the displayed images and the real world. Combiners can be realized through simple polarizing/non-polarizing beam splitter cubes, partial reflective concave mirrors, surface-relief gratings (SRGs) or holographic gratings (HGs) coupled waveguide (Fig. 1(b)). For the former two, a partially reflecting component is placed at an angle, leading to a larger form-factor. For SRGs- and HG-coupled waveguides, a thin-film SRG or HG is used as an in-coupled grating to guide the collimated displayed light into a flat waveguide, and then an out-coupled grating deflects the light toward user's eye. This allows a slim design and thus becomes a more reasonable approach for AR devices. SRGs are made of periodic submicron surface profile to allow beam deflection at large angle, while common HGs are made of isotropic materials with alternative slanted layers of high and low refractive indices. The angular bandwidth for a single HG is determined by the index contrast. As reported in [14], HGs based on dichromated gelatin can provide an index contrast as high as 0.15; however, this type of HG is sensitive to humidity, temperature and other environmental conditions, which makes it extremely unstable and causes defects in grating structure. Nowadays, most of display applications choose photo-polymers as recording media with index contrast around 0.035 [15]. As a result, the deflection has a high angle/ wavelength selectivity. This allows almost 100% transmittance of the background light; however, this also implies to a lower efficiency and lower acceptance angle for the displayed light, resulting in a smaller field of view (<5°) and higher energy consumption. To have a larger field of view while maintaining flat profile, multilayered HGs are exploited. This not only reduces the transmittance but also greatly increases the device cost. Toward this end, Pancharatnam-Berry deflectors (PBDs) and reflective polarization volume gratings (RPVGs), due to the inherent high index contrast (>0.15), can provide high efficiency over a large field of view (~15°) and wider spectral width, and have high potential to replace the conventional isotropic HGs.

In the following, we first review the basic operation principle and then discuss the recent development in PB optical elements.

2 Operation Principle

Pancharatnam–Berry phase optical elements (PBOEs) [16–36], also known as cycloidal diffractive waveplates (CDWs), are essentially patterned half-wave plates with spatially varying crystal-axis orientation (director). The underlying operation principles of PBOEs can be described by Jones matrices, assuming an input light as:

$$J_{\pm} = \frac{1}{\sqrt{2}} \begin{bmatrix} 1 \\ \pm i \end{bmatrix}, \tag{1}$$

where J_+ and J_- corresponds to left- and right-handed circularly polarized light (LCP and RCP), respectively. When passing through a half-wave plate at azimuthal angle ϕ, the output can be written as:

$$\begin{aligned} J'_{\pm} &= R(-\phi) \cdot W(\pi) \cdot R(\phi) \cdot \begin{bmatrix} 1 \\ \pm i \end{bmatrix} \\ &= \frac{1}{\sqrt{2}} \begin{bmatrix} \cos 2\phi & \sin 2\phi \\ \sin 2\phi & -\cos 2\phi \end{bmatrix} \begin{bmatrix} 1 \\ \pm i \end{bmatrix} = \begin{bmatrix} 1 \\ \mp i \end{bmatrix} e^{\pm 2i\phi}, \end{aligned} \tag{2}$$

where $R(\phi)$ and $W(\pi)$ are the Jones matrix representations of rotation and phase retardation, respectively. Eq. (2) indicates that when the incident light is circularly polarized, in addition to flipping the handedness, the circularly polarized input also accumulates a phase according to the azimuthal angle ϕ. This is very different from a conventional liquid crystal (LC) phase modulator, which utilizes the change in polar angle (or tilt angle) to modulate phase, resulting in a discontinuity at the boundary of 2π modulo. Instead, in the case of a PBOE phase modulation, since azimuthal angle is varying continuously across space, this mapping from azimuthal angle to phase allows a continuous phase change and therefore allows more drastic phase change without introducing discontinuity at the boundary of 2π and 0 modulo.

For a typical PBL, as Fig. 2(a) depicts, its director continuously changes along radial axis in a parabolic fashion. A PBD, as shown in Fig. 2(c), has a linearly changing director. In these distribution, the phase profile is effectively parabolic or linear so that its far-field behavior acts as a lens or a prism (blazed grating). We'd like to stress here the difference between PBL/PBDs and a Fresnel lens/prism array. Although they have a similar profile, PBOEs are continuous modulation of phase, while Fresnel lens/prism arrays are modulation in macroscopic shape of the material. The former must be modelled through diffraction while the later with Fresnel refraction. This causes a profound difference in wavelength dispersion. The diffraction-based modulation leads to a larger deflection angle at a longer wavelength, but the refraction-based modulation results in a larger deflection angle at a shorter wavelength. Meanwhile, Fresnel lenses/prism arrays have discontinuous structures that lead to limited resolution, scattering losses, and stray light. To obtain relatively high efficiency, traditional Fresnel lenses are made using multilevel high-resolution lithography techniques that are only affordable to most advanced research institutions [40]. The complexity of the technology renders it difficult to scale up the conventional Fresnel lenses both in sizes and fabrication quantities.

The other interesting property of PBOEs, as shown in Eq. (2), is that the phase profile of RCP and LCP have opposite signs. This indicates that RCP and LCP will acquire opposite phase profile. For PBLs, this corresponds to diverging and converging lens for the LCP and RCP beams, as Fig. 2(b) depicts, while for PBDs this means a positive and a negative deviation angle, as shown in Fig. 2(d).

Two major schemes can be exploited for driving a PBOE [33]: (1) Active driving: We can directly apply a voltage across the PBOE to switch the LC directors between spatially patterned waveplate (which acts as a lens for focusing/defocusing the circularly polarized input) to homeotropic plate (which can be treated as a transparent plate), as Fig. 3(a) depicts (only shows the case of a PBL, but also applies to PBDs). (2) Passive driving: We can add an external polarization rotator to select the input polarization between LCP and RCP to switch between the focusing and defocusing states, as Fig. 3(b) indicates. We refer to scheme I as active driving mode and scheme II as passive driving mode. In the active driving mode, the whole device consists of only a PBL and a circular polarizer on the input side. As for the passive driving mode, we need an extra fast-switching polarization rotator (e.g. a twisted-nematic (TN) LC cell or a ferroelectric LC cell) and a $\lambda/4$ film. It is noteworthy that in passive driving mode it is common to exploit liquid crystal polymer film instead of electrically responsive liquid crystal molecules so that the film thickness can be well-controlled and further optimization on efficiency can be made through director modulation in z axis (defined as the axis perpendicular to the substrate), as will be discussed in the following section.

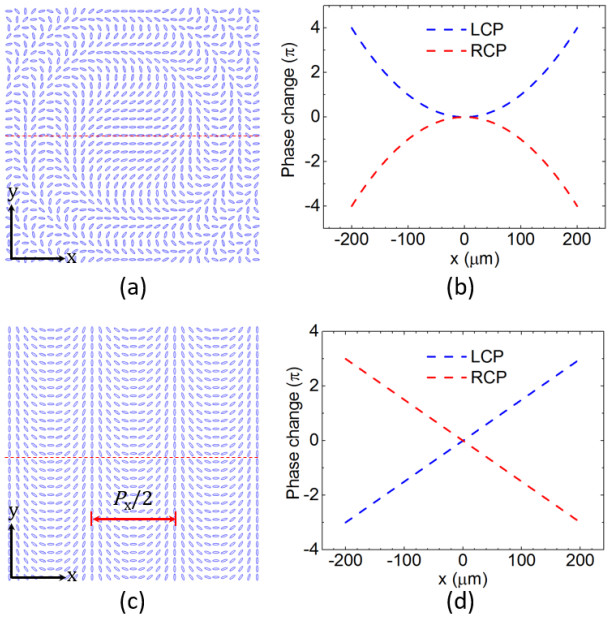

Figure 2: (a) Top view of a PPL: the direction of the LC optical axis changes radially. (b) The corresponding phase change along the dashed lines in (a). (c) Top view of a PBD: the direction of the LC optical axis changes longitudinally. (d) The corresponding phase change along the dashed lines in (c).

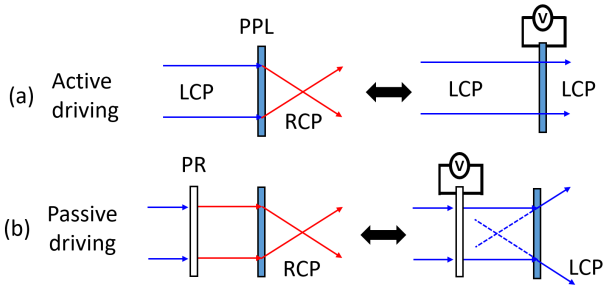

Figure 3: Two different driving methods: (a) active driving, in which a voltage is applied directly to the PBL, resulting in a switching between $f = f_{PBL}$ and $f \to \infty$; (b) Passive driving with a polarization rotator (PR) to select the input polarization, resulting in a switching between $f = f_{PBL}$ and $f = -f_{PBL}$.

3 Device fabrication and performance

To fabricate a PBOE [36], a thin film of photo-alignment material such as PAAD-72 (BEAM Co.), brilliant yellow or SD-1 is coated on to a substrate. For active driving mode, these substrates with transparent electrodes were first assembled to form a LC cell with a certain cell gap, and then subjected to interference exposure. For passive driving, since only one alignment layer is required, the coated substrates are directly subjected to interference exposure. An optical setup is shown in Fig. 4. The beam from a linearly polarized laser (UV, violet or blue) was split into two paths with a non-polarizing beam splitter (NPBS). They were then sent through a quarter wave plate (QWP) to generate two opposite-handed circularly polarized beams. One beam passed through a focusing lens L_0 to adopt a parabolic wave-front, and these two beams were then combined with the other NPBS. At the twice the focal length of L_0, the interfered patterns can then be recorded onto the LC cell. The optical setup for fabrication of PBDs is similar, with L_0 removed and an angle introduced between two arms to form a linear change in phase profile. After exposure of sufficient dosage, for active driving, the exposed cell will be filled with liquid crystal with appropriate birefringence (Δn) such that $d\Delta n \cong 0.5\,\lambda$. On the other hand, for passive driving, the exposed substrate will be used for spin-coating with diluted liquid crystal monomer such as RM257 or RMS03-001 (Merck). Then the substrate is dried and exposed with UV to form cross-linked liquid crystal polymer thin film.

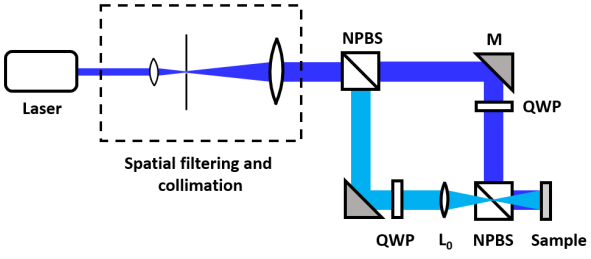

Figure 4: The setup for interference exposure process for a PBL. The beam from a linearly polarized laser is filtered and collimated and split into two paths with a non-polarizing beam splitter (NPBS). They pass through quarter wave plates (QWPs) to form two opposite-handed circularly polarized light beams. One of the beams (light blue) passes through a focusing lens L_0 to adapt a parabolic wavefront, and these two beams are then combined with the other NPBS. At the twice of the focal length of L_0, the interfered patterns can then be recorded onto the LC sample.

3.1 Response time

Figure 5 shows the experimental setup for measuring the switching time of an active-driving PBL. A laser source (e.g. Ar^+ laser, λ =514 nm) was focused and filtered with a pinhole and then collimated onto a circular polarizer. The PBL was placed at a position such that the light was focused into an aperture at the focal length of PBL. The light was then collected by a lens into the photodiode detector. When an appropriate voltage was applied, the LC directors were reoriented vertical to the substrates and thus the focal length became infinity. As a result, most of the light will be blocked by the aperture (dashed lines). For the measurement of PBDs, the aperture may be shifted from the center and aligned such that only at the voltage-off state the laser beam can fully pass through.

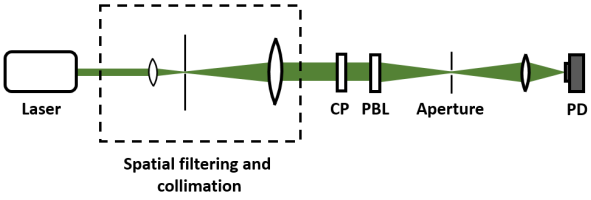

Figure 5: The measurement setup for an active driving PBL. The filtered and collimated green laser beam (514 nm) was polarized with a circular polarizer (CP) and then focused by the PBL through an aperture and then focused again into the photodiode detector (PD). When the voltage is applied, most of the light (dashed line) will be blocked by the small aperture.

Figure 6 shows the measured switching behaviors of a PBL. For a LC device, the relaxation time can be approximated by the following equation [37]:

$$\tau = \frac{\gamma_1}{K_{11}} \frac{d^2}{\pi^2}, \tag{3}$$

where γ_1/K_{11} stands for the visco-elastic constant of the employed LC mixture. This equation describes the response time of LC *director* reorientation, while the actual *optical* response time (transmittance change from 10% to 90%) is often faster. In our experiment with active driving mode, as shown in Fig. 6, the voltage-off process (relaxation from 7 V_{rms}) has a response time of 0.54 ms. The rise time can be shortened by increasing the applied voltage. At 7 V_{rms}, the measured rise time is 0.18 ms. Such a fast switching time originates from a relatively low visco-elastic constant of UCF-M37 (γ_1/K_{11} = 4.0 ms/μm^2 at 22°C) and thin cell gap (1.6 μm). Even though a faster response time can be obtained by further decreasing the cell gap, it will demand a higher Δn LC to satisfy the condition $d\Delta n \cong 0.5\,\lambda$. A high Δn LC exhibits a larger wavelength

dispersion, which in turn leads to a more pronounced efficiency loss, as will be discussed later. The same switching behavior holds for PBDs. For passive driving, the response time is determined by the polarization rotator. A thin TN polarization rotator can have a response time of 2 ms [41], while a ferroelectric polarization rotator usually has a response time of around 0.1 ms [42]. The major difference is that TN is a broadband polarization rotator.

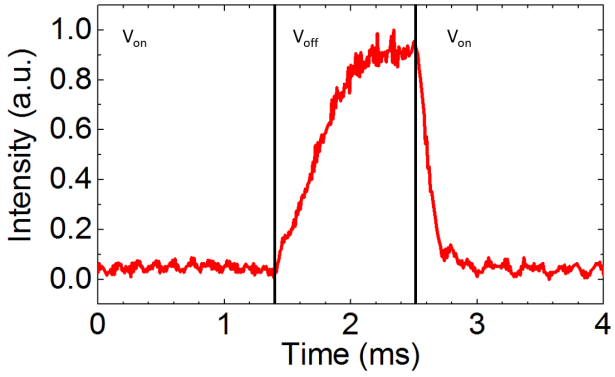

Figure 6: Upon releasing voltage from 7 V_{rms}, the PBL switches from$f \to \infty$ to $f = f_{PBL}$ and thus passing through the aperture. The switching time was 0.54 ms (V-off) and 0.18 (V-on).

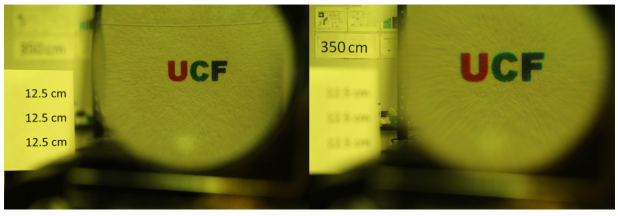

Figure 7: When looking into the PBL and the offset lens, the switching of voltage-on and voltage-off states upon PBL results in different image distances as shown above. The left photo shows the image when the PBL is in voltage-off state (image located at 12.5 cm), while the right photo shows the image in voltage-on state (image located at 350 cm).

To demonstrate the switching range and behavior, a simple system was set up, as shown in Fig. 7, where a PBL (f_{PBL} = 13 cm) was placed near a biconvex lens (as an offset lens, f_{bc} = 4 cm) to form a compound lens that switches between f_{off} = 3.06 cm and f_{on} = 4 cm. A circular polarizer was laminated onto the PBL. A printed "UCF" colored image was placed behind the compound lens slightly over 4 cm to produce an image distance switching of 12.5 cm (voltage-off state) and 350 cm (voltage-on state) as can be seen from the distance reference aside from the lens. This corresponds to a switching of 7.7 diopters. The image size for the switched-on and switched-off states is different due to the mismatched secondary principle plane. This can be easily corrected by sandwiching the PBL between two plano-convex lenses to form a symmetric configuration. For integration in depth-fused or light-field display devices, a smaller switching range (e.g., 3 diopters) is sufficient.

In Fig. 8, we demonstrated a 30-Hz 2-panel additive temporal-multiplexing light-field display based on a fast switching PBL with 16 view points in a square eye box of 8 mm by 8 mm. The PBL used in this case has a lens power of 1 diopter and switching time <1 ms. The rendering of light field follows the one as described in [5]. The display panel has a resolution of 401 ppi and was magnified with two plano-convex lenses with focal lens of 10 cm sandwiching the PBL lens and a circular polarizer to form a compact switchable lens. Thus, this lens can switch between two focal lengths of roughly 4.76 cm and 5 cm through applying a voltage of 8 V_{rms} (frequency= 1 kHz). The display was placed at roughly 5.1 cm away from the switchable lens, which was synchronized with the rendered image to reconstruct correct light field at different viewpoints with focus cues. During voltage-off frame Fig. 8(a) was displayed, while during voltage-on frame Fig. 8(b) was displayed. The resultant image was captured with a camera. When focusing at rear object A, object B became blurry as Fig. 8(c) shows, and when focusing at front object B, rear object A became blurry [Fig. 8(d)]. This method provides correct focus cue of the 3D objects with minimal resolution loss.

3.2 Achromatized efficiency

For practical applications, we examine here the efficiency (η) of a PBL, which is defined as the focused beam intensity divided by the total beam intensity with the input light being circularly polarized. In theory, η can be expressed as [38, 39]:

$$\eta = \sin^2\left(\frac{\pi \Delta n d}{\lambda}\right). \tag{4}$$

From Eq. (4), one can plot the wavelength dependent efficiency and results are shown in Fig. 9. Here the PBL is an LC cell with 1.6-μm-thick UCF-M37 (optimized at λ =512 nm, i.e., Δnd = 256 nm). Note that in this plot, the LC birefringence dispersion was modeled according to the equation below [43]:

$$\Delta n = G\frac{\lambda^2 \lambda^{*2}}{\lambda^2 - \lambda^{*2}}, \tag{5}$$

with G =2.15 × 10^{-6} nm^{-2} and λ^* = 241 nm through fitting the Δn dispersion data of UCF-M37.

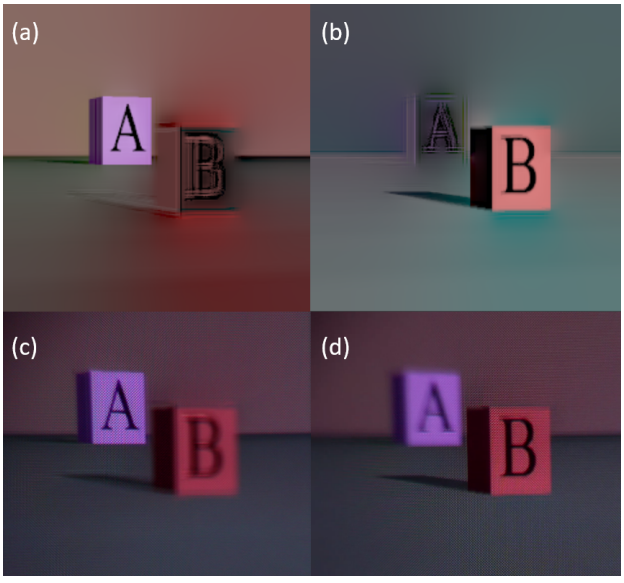

Figure 8: A 2-panel additive light field display based on PBL switchable lens. (a) The rendered subframe image when the lens is off. (b) The rendered subframe image when lens is activated. (c) The actual image captured with a camera focusing at rear object. (d) The actual image captured with a camera focusing at front object.

As can be seen in Fig. 9, the efficiency at normal incidence drops to below 90% at 450 nm and 650 nm, while high-efficiency performance across all visible wavelength is critical in many applications. Since PBOEs are essentially patterned half-wave plates, achromatization can be realized in a similar way, which is to introduce director modulation along z axis. As reported by Oh and Escuti [44], a dual-twist structure (Fig. 10(a)) can effectively widen the operation wavelength with over 95% efficiency. In this structure, the LC director along x-axis is the same as a regular PBOE, while along z-axis it twists to a certain degree Φ from bottom to half way across the film, and then twists back through the top. The efficiency η as a function

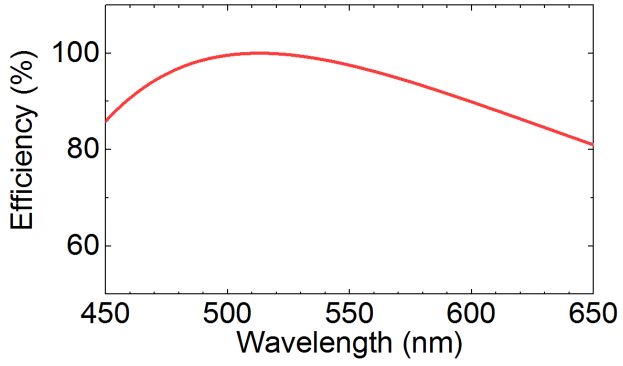

Figure 9: The wavelength dependent efficiency of PBL. In this spectral region, the efficiency is over 80%.

of twist angle Φ and phase retardation Γ can be described as [44]:

$$\eta = 1 - [\cos^2 \mathrm{X} + (\Phi^2 - \Gamma^2)\mathrm{sinc}^2 \mathrm{X}]^2, \tag{6}$$

where $\Gamma = \pi d\Delta n/\lambda$, $\mathrm{X} = \sqrt{\Phi^2 + \Gamma^2}$ and sincX=sin(X)/X.

In Fig. 10(b) we plot the efficiency for a dual-twist structure with d = 1.8 μm and Δn = 0.15. It shows high efficiency (>98%) across 450–650 nm wavelength region when the twist angle is at 70° (red solid line). To experimentally realize the 70° dual-twist structure, a carefully controlled amount of chiral dopant should be doped into the precursor for spin-coating. After photo-polymerization, a precursor with opposite handedness chiral dopant is spun-coated onto the polymerized layer and subjected to photo-polymerization again to form a dual-twist structure.

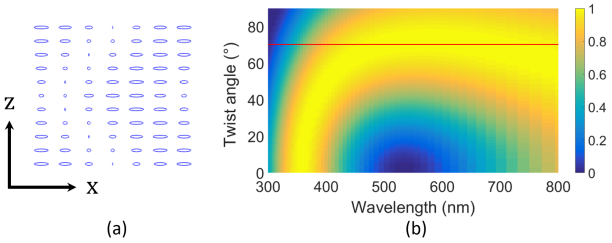

Figure 10: (a) The side view of an achromatized dual-twist PBOE. (b) The efficiency of a dual-twist PBOE (d = 1.8 μm, Δn = 0.15) with different twist angle across visible wavelength. It shows a >98% high efficiency across 450–650 nm when the twist angle is 70°.

3.3 Wavelength-dependent deflection and longitudinal chromatic aberration

Although the efficiency can be achromatized through the adoption of dual-twist structure, the deflection angle θ in a single PBD is always wavelength-dependent. It can be described simply as:

$$P_x/2 = \lambda/\sin\theta, \tag{7}$$

where P_x is the distance along x axis where LC directors rotate by 360°, as shown in Fig. 2(c). This indicates that, in contrast to a prism, light with a shorter wavelength deflects less than that with a longer wavelength. By treating PBL as a period-changing PBD, it is straightforward to see that, for a given PBL, the focal length can be approximated by:

$$f \propto \frac{1}{\lambda}. \tag{8}$$

This approximation clearly shows that the longitudinal chromatic aberration (LCA) is the opposite of a conventional lens or a Fresnel lens. For practical purposes, in Fig. 11, the LCA as a function of lens power K (defined as $K = 1/f$ in diopter, or m^{-1}) at 589 nm was plotted for an N-BK7 bi-convex lens and a PBL. The longitudinal chromatic aberration is expressed here as ΔK, defined as K at λ =656 nm minus K at λ =486 nm. One can see that PBLs have significantly stronger negative longitudinal chromatic aberration in comparison with that of a conventional concave/convex lens. At K = 25 D (that is, a focal length of 4 cm), PBL has a ΔK of −7.22, while N-BK7 has a ΔK of 0.39. For depth-fused display, to match accommodation, a switching of 3 diopters is preferred; for PBL, this corresponds to a ΔK of −0.86. Compensation can be easily applied, e.g., with a 20-D bias lens made of N-BK7, resulting in a total of ΔK = −0.55.

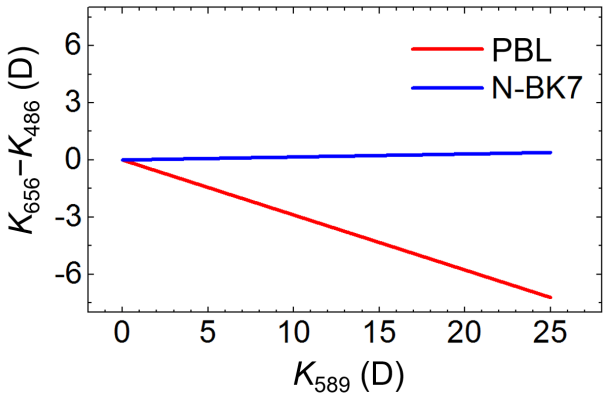

Figure 11: Comparing the longitudinal chromatic aberration between a PBL and an N-BK7 biconvex lens. The optical power of PBL is significantly dependent on the wavelength.

3.4 Going toward larger deflection angle

For the application as a waveguide coupler in AR, due to the limitation of total internal reflection (TIR), it is critical to have a ~55° deflection angle in the waveguide. This allows the display light to be deflected and guided toward the viewing region through TIR and deflect again toward the user's eye. For a PBD with small deflection angle, it is reasonable to assume the linear phase profile is acquired through an infinitesimally-thin PBD. However, when the deflection angle is large, the change of wave-front within the PBD becomes non-negligible. As reported by Cheng et al. [45, 46], at a large deflection angle, say 50°, the efficiency drops quickly to below 20%. A solution to large-angle high-efficiency PBDs, like the case of achromatization, is to introduce a certain twist into the PBD. Instead of describing the vertical twist in terms of twist angle, we define the vertical pitch (p_z) to be the distance along z axis when the LC directors rotate 360°.

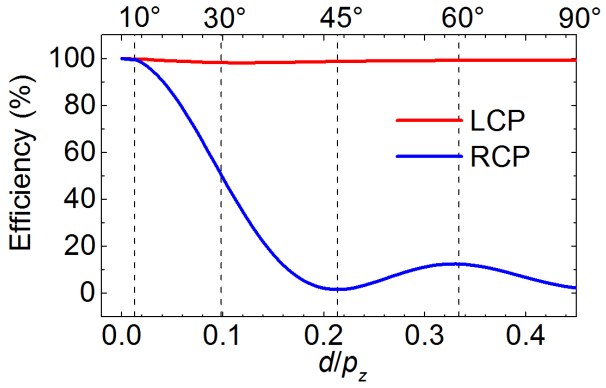

Figure 12: An example of a large-angle high-efficiency PBD with d = 1.37 μm and Δn = 0.2, showing the requirement on p_z for different deflection angle to maintain a high-efficiency deflection for LCP. Due to the asymmetry, for RCP the efficiency drops quickly to zero at 45° deflection. At this deflection angle, the RCP traverses through PBD without deflection and changing its polarization state.

As shown in Fig. 12, to maintain high diffraction efficiency at a desired angle (labeled on top of the plot) of deflection for, say LCP, the corresponding d/p_z should be incorporated. In this specific case, d = 1.37 μm and Δn = 0.2. This twist introduces an asymmetry into the system, and results in an asymmetric deflection efficiency for LCP and RCP. At a deflection angle of 45°, the efficiency for RCP drops to zero, and therefore a RCP input will pass through the PBOE without deflection or change of polarization state. Along this route, Gao et al. [34] demonstrated a high-efficiency 40° deflector with dual-twist structure, and therefore the result resembles that of the non-twist PBD, i.e., same high efficiency deflection in opposite direction for RCP and LCP. Though PBDs with proper twisting angle allow good in- and out-coupling for waveguide-based AR device, as a phase-based grating, it also affects the real-world light on the waveguide output side, since the modulation is phase-based.

4 Reflective polarization volume gratings

In addition to transmission-type deflector, a reflective polarization volume grating (RPVG) [35, 47], which incor-

porates a higher degree of twist along z-axis (i.e., much smaller p_z, as shown in Fig. 13(a)) can be configured as well. Although its device structure is somewhat similar to that of large-angle PBDs described above, the deflection mechanism is completely different. Instead of modulating the phase of an input light, a RPVG deflects light through Bragg reflection (or slanted multilayer reflection). This difference manifests when we take a closer look into the efficiency as a function of film thickness (d). As shown in Fig. 13(b), we compare a 40° deflection at 550 nm for a PBD and a RPVG with $\Delta n = 0.2$ at different film thickness. Note that in this case the p_z for PBD is 8.05 μm for high-efficiency and large-angle deflection, while for RPVG it is 0.4 μm. For PBDs, the efficiency drops as d increases over the first optimal thickness, while for a RPVG the efficiency increases monotonically with thickness (number of layers) and then gradually saturates. When d ≥ 2.8 μm, the efficiency reaches 98%.

In contrast to conventional HGs, RPVGs can have much higher index contrast and therefore exhibits higher efficiency and larger acceptance angle. One major difference between RPVGs and HGs is the polarization selectivity. Since HGs are essentially slanted multi-layers made of different isotropic materials, they are polarization-independent. On the other hand, RPVGs are uniaxial crystals with slanted helical axis, allowing deflection only for one circularly polarized light while the other polarization will transmit through. This not only increases the overall transmittance of the real-world light but also allows the realization of a single-panel AR headset. As shown in Fig. 14, Weng et al. [35] proposed an exemplary setup, by switching between LCP and RCP through a polarization rotator disposed on the output side of the display panel, light can be guided to the user's left and right eyes in a time sequential manner. Therefore, it reduces the number of display panel needed for the headset, allowing a smaller form factor.

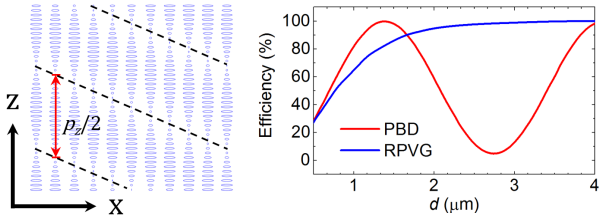

Figure 13: (a) A schematic illustration of a RPVG. The twist of director in both x and z axis result in an effective slanted multi-layer structure for the circular polarized light with same handedness. (b) A comparison between HLPBD and RPVG with deflection angle of 40° at 550 nm, in a glass of n = 1.57. The material has $\Delta n = 0.2$ and the vertical pitch p_z are 8.05 μm and 0.4 μm for PBD and RPVG, respectively. By increasing film thickness, the efficiency of HLPBD oscillates, while for RPVG, it grows monotonically.

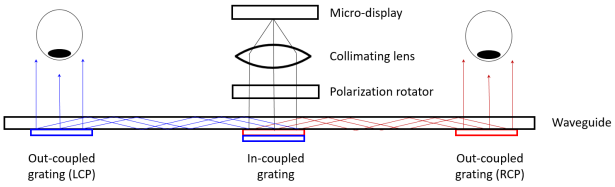

Figure 14: A schematic setup for single-panel AR device. The output from micro-display is collimated and sent through a polarization rotator that switches quickly between LCP (blue) and RCP (red). Due to the selectivity of RPVG, the displayed image can be sent to the left eye and right eye in a time-sequential fashion.

5 Conclusion

We have reviewed the recent progress on Pancharatnam–Berry phase holographic optical elements and emphasized on practical applications. The unique properties of PB optical elements allow fast and high-efficiency switchable lenses for modulating the image distance. By introducing twist structure along z-axis, high efficiency across the entire visible wavelength can be obtained. Based on this fast switching lens we demonstrated a prototype of additive temporal-multiplexing light field display that provided correct focus cue. For the application on thin waveguide couplers in AR devices, large-angle high-efficiency beam deflection can be achieved through matching the phase condition, by properly controlling the twist angle, both transmissive and reflective large-angle deflectors can be realized. Overall, recent developments in PBOEs show promising potentials for accommodation-matched and highly efficient head-mounted display devices.

References

[1] D. Lanman and D. Luebke, "Near-eye light field displays," ACM Trans. Graph. **32**(6), 1–10 (2013).

[2] H. S. Park, R. Hoskinson, H. Abdollahi, and B. Stoeber, "Compact near-eye display system using a superlens-based microlens array magnifier," Opt. Express **23**(24), 30618-30633 (2015).

[3] C.-K. Lee, S. Moon, S. Lee, D. Yoo, J.-Y. Hong, and B. Lee, "Compact three-dimensional head-mounted display system with Savart plate," Opt. Express **24**(17), 19531-19544 (2016).

[4] F. C. Huang, K. Chen, and G. Wetzstein, "The light field stereoscope: immersive computer graphics via factored near-eye light field displays with focus cues," ACM Trans. Graph. **34**(4), 60 (2015).

[5] S. Lee, C. Jang, S. Moon, J. Cho, and B. Lee, "Additive light field displays: realization of augmented reality with holographic optical elements," ACM Trans. Graph. **35**(4), 60 (2016).
[6] S. Liu and H. Hua, "A systematic method for designing depth-fused multi-focal plane three-dimensional displays," Opt. Express **18**(11), 11562–11573 (2010).
[7] S. Ravikumar, K. Akeley, and M. S. Banks, "Creating effective focus cues in multi-plane 3D displays," Opt. Express **19**(21), 20940–20952 (2011).
[8] H. Ren and S. T. Wu, *Introduction to Adaptive Lenses* (Wiley, 2012).
[9] S. Ravikumar, K. Akeley, and M. S. Banks, "Creating effective focus cues in multi-plane 3D displays," Opt. Express **19**(21), 20940–20952 (2011).
[10] Y. H. Lee, F. Peng, and S.T. Wu, "Fast-response switchable lens for 3D and wearable displays," Opt. Express **24**(2), 1668-1675 (2016).
[11] S. Liu and H. Hua, "A systematic method for designing depth-fused multi-focal plane three-dimensional displays," Opt. Express **18**(11), 11562–11573 (2010).
[12] B. T. Schowengerdt and E. J. Seibel, "True 3-D scanned voxel displays using single or multiple light sources," J. Soc. Inf. Disp. **14**(2), 135 (2006).
[13] S. W. Lee and S. S. Lee, "Focal tunable liquid lens integrated with an electromagnetic actuator," Appl. Phys. Lett. **90**(12), 121129 (2007).
[14] T. Rasmussen, "Overview of high-efficiency transmission gratings for molecular spectroscopy," Spectroscopy **29**(4), 32–39 (2014).
[15] F. Bruder, T. Fäcke, R. Hagen, D. Hönel, E. Orselli, C. Rewitz, T. Rölle, and G. Walze, "Diffractive optics with high Bragg selectivity: volume holographic optical elements in Bayfol®HX photopolymer film," Proc. SPIE **9626**, 96260T (2015).
[16] E. Hasman, V. Kleiner, G. Biener, and A. Niv, "Polarization dependent focusing lens by use of quantized Pancharatnam–Berry phase diffractive optics," Appl. Phys. Lett. **82**(3), 328–330 (2003).
[17] S. Pancharatnam, "Generalized theory of interference and its applications," Proc. Indian Acad. Sci., Sect. A **44**(5), 247–262 (1956).
[18] M. V. Berry, "Quantal phase factors accompanying adiabatic changes," Proc. R. Soc. London, Ser. A **392**(1802), 45–57 (1984).
[19] L. Marruccia, C. Manzo, and D. Paparo, "Pancharatnam-Berry phase optical elements for wave front shaping in the visible domain: Switchable helical mode generation," Appl. Phys. Lett. **88**(22), 221102 (2006).
[20] Y. Ke, Y. Liu, J. Zhou, Y. Liu, H. Luo, and S. Wen, "Optical integration of Pancharatnam-Berry phase lens and dynamical phase lens," Appl. Phys. Lett. **108**(10), 101102 (2016).
[21] B. Piccirillo, M. Florinda P. L. Marrucci, and E, Santamato, "Flat polarization-controlled cylindrical lens based on the Pancharatnam–Berry geometric phase," Eur. J. Phys. **38**(3), 034007 (2017).
[22] N. V. Tabiryan, S. V. Serak, D. E. Roberts, D. M. Steeves, and B. R. Kimball, "Thin waveplate lenses of switchable focal length - new generation in optics," Opt. Express **23**(20), 25783-25794 (2015).
[23] N. V. Tabiryan, S. V. Serak, D. E. Roberts, D. M. Steeves, and B. R. Kimball, "Thin waveplate lenses: new generation in optics," Proc. SPIE **9565**, 956512 (2015).
[24] A. M. W. Tam, F. Fan, H. S. Chen, D. Tao, V. G. Chigrinov, H. S. Kwok, and Y. S. Lin, "Continuous nanoscale patterned photoalignment for thin film Pancharatnam-Berry phase diffractive lens," SID Int. Symp. Digest Tech. Papers **46**(S1), 8 (2015).
[25] K. Gao, H. H. Cheng, A. K. Bhowmik, and P. J. Bos, "Thin-film Pancharatnam lens with low f-number and high quality," Opt. Express **23**(20), 26086–26094 (2015).
[26] N. Tabiryan, D. Roberts, E. Serabyn, D. Steeves, and B. Kimball, "Superlens in the skies: liquid-crystal-polymer technology for telescopes," (SPIE Newsroom 2016), http://spie.org/newsroom/6317-superlens-in-the-skies-liquid-crystal-polymer-technology-for-telescopes?ArticleID=x117044.
[27] N. V. Tabiryan, S. V. Serak, S. R. Nersisyan, D. E. Roberts, B. Ya. Zeldovich, D. M. Steeves, and B. R. Kimball, "Broadband waveplate lenses," Opt. Express **24**(7) 7091-7102 (2016).
[28] L. De Sio, D. Roberts, Z. Liao, S. Nersisyan, O. Uskova, L. Wickboldt, N. Tabiryan, D. Steeves, B. Kimball, "Digital polarization holography advancing geometrical phase optics," Opt. Express , **24**(16), 18297-18306, (2016).
[29] N. Tabiryan, D. Roberts, D. Steeves, and B. Kimball, "4G Optics: New technology extends limits to the extremes," Photonics Spectra **51**(3), 46–50 (2017).
[30] C. Provenzano, P. Pagliusi, and G. Cipparrone, "Highly efficient liquid crystal based diffraction grating induced by polarization holograms at the aligning surfaces," Appl. Phys. Lett. **89**(12), 121105 (2006).
[31] H. Sarkissian, S. V. Serak, N. V. Tabiryan, L. B. Glebov, V. Rotar, and B. Ya. Zeldovich, "Polarization-controlled switching between diffraction orders in transverse-periodically aligned nematic liquid crystals," Opt. Lett. **31** (15), 2248-2250 (2006).
[32] S. R. Nersisyan, N. V. Tabiryan, D. M. Steeves, and B. Kimball, "Optical axis gratings in liquid crystals and their use for polarization insensitive optical switching," J. Nonlinear Opt. Phys. Mater., **18**(1), 1–47 (2009).
[33] N. V. Tabiryan, S. R. Nersisyan, D. M. Steeves, and B. R. Kimball, "The promise of diffractive waveplates," Opt. Photonics News **21**, 41–45 (2010).
[34] K. Gao, C. McGinty, H. Payson, S. Berry, J. Vornehm, V. Finnemeyer, B. Roberts, and P. Bos, "High-efficiency large-angle Pancharatnam phase deflector based on dual-twist design," Opt. Express **25**(6), 6283-6293 (2017).
[35] Y. Weng, D. Xu, Y. Zhang, X. Li, and S.-T. Wu, "Polarization volume grating with high efficiency and large diffraction angle," Opt. Express **24**(16), 17746-17759 (2016).
[36] J. Kim, Y. Li, M. N. Miskiewicz, C. Oh, M. W. Kudenov, and M. J. Escuti, "Fabrication of ideal geometric-phase holograms with arbitrary wavefronts," Optica **2**(11), 958–964 (2015).
[37] D. K. Yang and S. T. Wu, *Fundamental of Liquid Crystal Devices* (Wiley, 2006).
[38] S. R. Nersisyan, N. V. Tabiryan, D. M. Steeves, and B. R. Kimball, "The principles of laser beam control with polarization gratings introduced as diffractive waveplates," Proc. SPIE **7775**, 77750U (2010).
[39] H. Chen, Y. Weng, D. Xu, N. V. Tabiryan, and S.-T. Wu, "Beam steering for virtual/augmented reality displays with a cycloidal diffractive waveplate," Opt. Express **24**(7), 7287-7298 (2016).
[40] R. Hyde and S. Dixit, "A giant leap for space telescopes," Lawrence Livermore National Laboratory Science & Technology Review, pp. 12-18 (March 2003).

[41] A. Chao, K. T. Huang, C. W. Tsai, Y. W. Hung, H. F. Cheng, W. Yeh, C. H. Yu, and H. H. Wu, "The fastest response TN-type TFT LCD of the world likes OCB level," SID Int. Symp. Digest Tech. Papers **38**(1), 603–606 (2007).

[42] A. Srivastava, V. Chigrinov, and H. S. Kwok, "Ferroelectric liquid crystals: Excellent tool for modern displays and photonics," J. Soc. Inf. Disp. **23**(6), 253-272 (2015).

[43] S.-T. Wu, "Birefringence dispersions of liquid crystals," Phys. Rev. A. **33**(2), 1270–1274 (1986).

[44] C. Oh and M. J. Escuti, "Achromatic diffraction from polarization gratings with high efficiency," Opt. Lett. **33**(20), 2287–2289 (2008).

[45] H. Cheng, A. K. Bhowmik, and P. J. Bos, "Analysis of a dual-twist Pancharatnam phase device with ultrahigh-efficiency large-angle optical beam steering," Appl. Opt. **54**(34), 10035-10043 (2015).

[46] H. Cheng, A. K. Bhowmik, and P. J. Bos, "Concept for a transmissive, large angle, light steering device with high efficiency," Opt. Lett. **40**(9), 2080-2083 (2015).

[47] J. Kobashi, H. Yoshida, and M. Ozaki, "Planar optics with patterned chiral liquid crystals," Nat. Photonics **10**(6), 389–392 (2016).